conversion rates in the system studied here can be explained by intramolecular phenomena that might result from the intermolecular effects such as packing differences. X-ray crystallographic analyses of both salts at different temperatures showed that the faster spin interconversion is accompanied by smaller metal to ligand bond length changes in the BPh_4^- salt as compared to the PF_6^- salt. We conclude that the activation energy ΔE_a for the BPh_4^- salt is smaller than that for the PF_6^- salt, and this implies the more rapid spin interconversion in the BPh_4^- salt.

Acknowledgment. We thank Prof. P. Gütlich (Johannes Gutenberg-Universität) and Prof. M. Sorai (Osaka University) for their helpful discussions.

Supplementary Material Available: Tables SI-SXXV, listing X-ray data collection parameters, derived hydrogen positions, thermal parameters, bond distances and angles, and magnetic susceptibility data, and Figures SI-SX, showing molecular structures and packing diagrams (32 pages); tables of calculated and observed structure factors (63 pages). Ordering information is given on any current masthead page.

Contribution from the Department of Chemical Engineering, University of Patras, and Institute of Chemical Engineering and High Temperature Chemical Processes, P.O. Box 1239, GR-26110 Patras, Greece, and Department of Chemistry, Bergakademie Freiberg, D-O-9200 Freiberg, Germany

Thermal Analysis and Raman Spectroscopic Measurements on the Scandium Iodide–Cesium Iodide System

M. M. Metallinou,[1a] L. Nalbandian,[1a] G. N. Papatheodorou,*[,1a] W. Voigt,[1b] and H. H. Emons[1b]

Received March 14, 1991

The phase diagram of the ScI_3–CsI system has been determined and the existence of two solid compounds, Cs_3ScI_6 and $Cs_3Sc_2I_9$, has been established. The Raman spectra of molten ScI_3–CsI mixtures containing up to 60 mol % ScI_3 have been measured at temperatures up to 700 °C. The temperature dependence of the Raman spectra of polycrystalline Cs_3ScI_6 and $Cs_3Sc_2I_9$ compounds from ambient temperatures to temperatures above melting have also been measured. The data are discussed in terms of the possible species formed in the melt mixtures. It is suggested that two predominant ionic species in equilibrium, $ScI_6^{3-} \rightleftharpoons ScI_4^- + 2I^-$, prevail in the melt. A third binuclear Sc species is also present at high ScI_3 concentrations. The Raman frequencies attributed to the ionic species are as follows: for ScI_6^{3-}, $\nu_1 = 119 \pm 1$ cm^{-1}, $\nu_2 = 67 \pm 2$ cm^{-1} ($\nu_5 \approx 80$ cm^{-1}); for ScI_4^-, $\nu_1 = 129 \pm 1$ cm^{-1}, $\nu_2 = 37 \pm 3$ cm^{-1}, $\nu_4 = 54 \pm 3$ cm^{-1}. The Raman spectra of vapors over an equimolar ScI_3–CsI mixture have been measured at 800 °C, and the observed bands at 127 ± 1 and 153 ± 1 cm^{-1} were assigned to the ν_1 stretching frequencies of the ScI_4 tetrahedra in the $CsScI_4$(g) molecule and of the ScI_3(g) molecule, respectively.

Introduction

The structural and thermodynamic properties of binary melts of the type MX_3–AX (X = halide, A = alkali metal, M = trivalent metal) are strongly dependent on the physicochemical properties of the trivalent salts.[2] Studies of binaries containing high-melting MX_3 salts are very limited, mainly due to experimental difficulties. Lanthanide and actinide halides, including the halides of yttrium and scandium, belong to this category. The practical interest for studying these mixtures arises from their use as additives in high-intensity-discharge mercury lamps.[3]

Phase diagrams for most of the above systems are available.[4-6] Calorimetric enthalpies of mixing and/or emf measurements have been performed on the systems YCl_3–ACl,[7] $LaCl_3$–ACl,[8,9] $CeCl_3$–ACl,[9,10] $GdCl_3$–ACl[11] (A = Li, Na, K, Rb, Cs) and $PrCl_3$–ACl[12] (A = Na, K). The results indicate that $LnCl_6^{3-}$ species stabilize the melt in the alkali-metal halide rich region for A = K, Rb, and Cs. Enthalpies of mixing have also been obtained for $LnCl_3$–NaCl (Ln = La, Ce, Nd, Sm, Dy, Er, Yb),[11] as well as $NdBr_3$–NaBr and NdI_3–NaI systems.[11] Electrical conductivity measurements of the LnX_3–AX (A = Na, K, Cs) mixtures indicate "complex" formation at the concentration of the compounds shown in the corresponding phase diagrams.[13,14] Further information for understanding the melt structure is given by combining thermodynamic measurements with spectroscopic techniques.[2] Thus Raman spectroscopic studies on the systems YCl_3–ACl (A = Cs, K, Li),[15] $LaCl_3$–KCl,[16,17] and $LaCl_3$–CsCl[17] have provided concrete evidence for the formation of YCl_6^{3-} and $LaCl_6^{3-}$ configurations in alkali-metal chloride rich mixtures.

This work was aimed at investigating the thermodynamic and structural properties of the ScI_3–CsI system. The phase diagram has been calculated from DTA measurements, and the Raman spectra of the liquid mixtures and the solid compounds formed have been measured at various temperatures.

Experimental Section

Scandium iodide was kindly provided by Dr. T. Russel of General Electric (Cleveland, OH) and used without further treatment. Cesium iodide was purchased from Fluka and was further dehydrated by heating at 100 °C under vacuum for several hours. All anhydrous materials were handled in sealed fused silica containers and/or in an inert atmosphere of a glove box having water content of less than 1 ppm.

For the DTA measurements, almost identical containers made of vitreous silica tubing (6 mm o.d., 4 mm i.d.) were used. The appropriate salt mixture with a total mass of about 80 mg was added, and the container was sealed under vacuum with the use of a propane/oxygen torch. The total length of each sealed container was approximately 12 mm. A similar empty container was used as a reference sample. DTA mea-

(1) (a) University of Patras and ICE/HT. (b) Bergakademie Freiberg.
(2) (a) Brooker, H. M.; Papatheodorou, G. N. In *Advances in Molten Salt Chemistry*, Mamantov, G., Ed.; Elsevier: New York, 1983; Vol. 5, pp 27-165, (b) Papatheodorou, G. N. In *Comprehensive Treatise of Electrochemistry*; Conway, B. E.; Bockris, J. O'M.; Yeager, E., Eds.; Plenum Press: New York, 1983; Vol. 5, pp 399-461.
(3) Van Erk, W.; Rietveld, T. *Philips J. Res.* **1987**, *42*, 102.
(4) *Phase Diagrams for Ceramists*; The American Ceramic Society: Westerville, OH, 1983; Vol. V.
(5) Kutscher, J.; Schneider, A. Z. *Anorg. Allg. Chem.* **1974**, *408*, 135.
(6) Krokhina, A. G.; Andrachnikova, A. P.; Strekachinskij, A. B.; Krokhin, V. A. *Zh. Neorg. Khim.* **1980**, *25*, 1624; *Russ. J. Inorg. Chem. (Engl. Transl.)* **1980**, *25*, 901.
(7) Papatheodorou, G. N.; Woernes, O.; Østvold, T. *Acta Chem. Scand.* **1979**, *A33*, 173.
(8) Papatheodorou, G. N.; Østvold, T. *J. Phys. Chem.* **1974**, *78*, 181.
(9) Papatheodorou, G. N.; Kleppa, O. J. *J. Phys. Chem.* **1974**, *78*, 176.
(10) Egan, J. J.; Bracker, J. *J. Chem. Thermodyn.* **1974**, *6*, 9.
(11) Dienstbach, F.; Blachnik, R. *Z. Anorg. Allg. Chem.* **1975**, *412*, 97.
(12) Iwadate, Y.; Igarashi, K.; Mochinaga, J. *J. Electrochem. Soc.* **1986**, *133*, 1162.
(13) Kutscher, J.; Schneider, A. *Z. Anorg. Allg. Chem.* **1972**, *389*, 157.
(14) Foerthmann, R.; Vogel, G.; Schneider, A. *Z. Anorg. Allg. Chem.* **1969**, *367*, 19.
(15) Papatheodorou, G. N. *J. Chem. Phys.* **1977**, *66*, 2893.
(16) Maroni, V. A.; Hathaway, E. J.; Papatheodorou, G. N. *J. Phys. Chem.* **1974**, *78*, 1134.
(17) Papatheodorou, G. N. *Inorg. Nucl. Chem. Lett.* **1975**, *11*, 483.

0020-1669/91/1330-4260$02.50/0

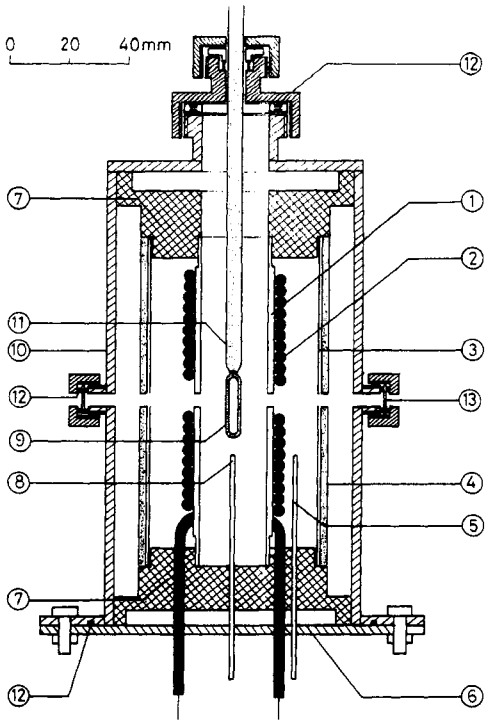

Figure 1. Vertical cross section of the optical furnace. Key: (1) central core, nickel alloy grade 600 (Tubesales), o.d. = 25.40 mm, i.d. = 22.10 mm; (2) heating wire (ARI Industries, 1HM-1258 type, o.d. = 4 mm, total resistance ≈ 3 Ω); (3) nickel foil (Goodfellow), thickness = 0.025 mm; (4) quartz tube supporting the nickel foil, o.d. = 50 mm, i.d. = 46 mm; (5) controlling thermocouple, Ni–Cr/Ni–Al; (6) bottom flange plate, stainless steel; (7) ceramic plates (Stenan, Hoechst-CeramTec); (8) measuring thermocouple, Ni–Cr/Ni–Al; (9) liquid-phase cell; (10) outer chamber, stainless steel; (11) quartz handle; (12) viton O-rings; (13) fused silica window. The laser light travels on the plane of the drawing, through the two shown windows, diameter 5 mm. The scattered radiation is detected at 90° to the incident laser light through a 30-mm window. Inside the outer chamber, vacuum ($\sim 10^{-5}$ Torr) is applied with the use of an adaptor on the rear side, in the bottom half of the furnace. The vacuum and the Ni reflecting foil minimize the heat loss giving a temperature gradient along the 2-cm-long Raman cell of ~2 °C at 700 °C.

surements were performed with a DSC-2000 (SETERAM) instrument, equipped with a crucible holder set. Sample and reference containers were placed in platinum crucibles inside the holder. Temperature was measured with Pt/Pt+Rd10 thermocouples and the heating and cooling cycles were recorded at a rate of 2 K/min. All samples were heated above their melting points and quenched before the DTA runs. Only the heating curves were used for the determination of phase-transition temperatures because of the supercooling effect present in the cooling curves. Powder X-ray diffraction patterns were obtained from each sample after the DTA measurements. A vertical-reflection-mode diffractometer (Philips PW-1050/70) with a graphite monochromator and Co Kα radiation was used. Patterns were recorded over the range $2° < 2\theta < 90°$ at a goniometer speed of 0.5°/min. During the X-ray measurements, the salt was placed in a small chamber filled with N_2 and covered with polythene foil in order to protect it from the atmospheric moisture.

Raman spectra of solids and melts were excited with the 647.1-nm line of a Kr^+ laser. The scattered radiation was analyzed at 90° with a SPEX 1403 double monochromator and measured with an RCA (C 31034) photomultiplier tube and EG&G/ORTEC photon-counting (Model 9315) and rate meter (Model 9349) electronics.

An optical furnace specially constructed for high-temperature Raman spectroscopy was used. Vacuum ($\sim 10^{-5}$ Torr) and nickel reflecting foil were used for thermal insulation and for achieving small temperature gradients. Figure 1 shows a drawing of the furnace, which has been described in more detail elsewhere.[18]

The molten salt samples were contained under vacuum in sealed vitreous silica tubing (4 mm o.d., 2 mm i.d.). The samples were clear yellow reddish liquids and show a slight absorption of the 647.1-nm laser line. In certain samples during sealing small amounts of iodine vapors were formed by decomposition of ScI_3 powder stuck on the tube surface. Relative to the bulk liquid sample, the decomposition was quantitatively negligible and did not affect the melt composition. Dissolution however of I_2 into the melt resulted in dark red solutions that strongly absorbed the 647.1-nm line and drastically reduced the scattered Raman intensity. This difficulty was surpassed by adding a small quantity of Sc metal into each sample, which reacted and cleared the melt of the I_2 vapors. For the gas-phase Raman studies, cylindrical vitreous silica cells (18 mm o.d., 16 mm i.d., 50 mm long) were used and the spectra were excited with the 488.0-nm Ar^+ laser line.

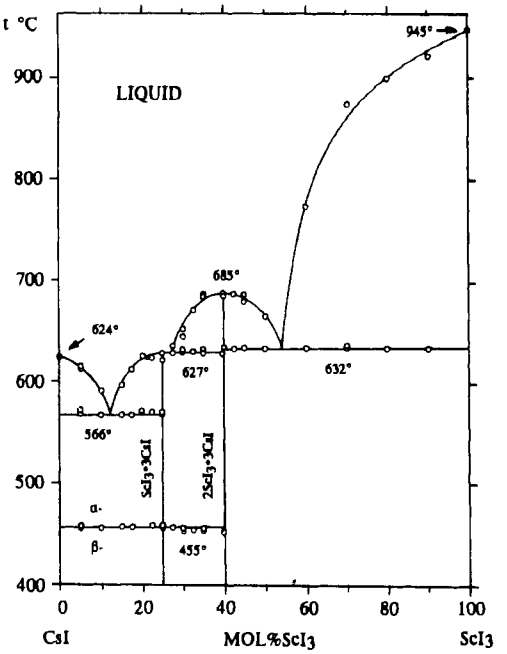

Figure 2. Phase diagram of the binary system ScI_3–CsI.

The melt and vapor spectra were recorded by using the two polarization configurations VV and HV. For the spectra of the polycrystalline solids the polarization of the incident radiation was randomly rotated by the material resulting in a common unpolarized–vertical (UV) configuration for both the VV and HV configurations.

Results and Discussion

Thermal Analysis and X-ray Diffraction. Table A (supplementary material) lists phase-transition temperatures in the ScI_3–CsI system determined from DTA curves. The melting point of ScI_3 was found to be 945 ± 1 °C (lit. values:[19] 945 ± 8 and 952 °C). An indirect determination of the melting point at 952 ± 1 °C has been recently made[20] based on drop-calorimetric experiments for stepwise enthalpy increments between 4 and 9 K.

From the data presented in Table A, the phase diagram shown in Figure 2 was derived. The existence of two solid compounds, $ScI_3{\cdot}3CsI$ ($^1/_3$) (mp = 627 ± 1 °C) and $2ScI_3{\cdot}3CsI$ ($^2/_3$) (mp = 684 ± 1 °C) has been established. A eutectic point (eu_1 = 566 °C) is observed between CsI and $ScI_3{\cdot}CsI$. When ScI_3 is added to the $ScI_3{\cdot}3CsI$ compound, no freezing point depression is observed. The melting point of the $^1/_3$ compound coincides with the eutectic temperature (eu_2 = 627 °C), which, according to our results, should form between the $^1/_3$ and $^2/_3$ compounds. Another eutectic point (eu_3 = 632 °C) is also formed between $2ScI_3{\cdot}3CsI$ and ScI_3. The presence of the two compounds has been verified by X-ray analysis. Data are given in Table B of the supplementary material. The phase diagram of the ScI_3–CsI system represents a continuation of the trends already observed in the ScI_3–AI (A = Na, K, Rb) series.[6] The system ScI_3–NaI is of the eutectic type, while in the ScI_3–KI system the $^1/_3$ compound is formed.

(18) Metallinou, M. M. Thesis, Department of Chemical Engineering, University of Patras, Patras, Greece, 1991.

(19) *Gmelin Handbuch der Anorganischen Chemie C6* (*System No. 39*); Springer: Berlin, 1978.

(20) O'Hare, P. A. G.; Johnson, G. K.; Tasker, I. R.; Flotow, H. E.; Struck, C. W. *J .Chem. Thermodyn.* **1987**, *19*, 77.

Table I. Raman Frequencies (cm^{-1}) Observed from the ScI_3–CsI Melt up to 60 mol % ScI_3

Raman frequency							
10%	17%	25%	34%	42%	50%	60%	assignment
			37 ± 3 vw, d	37 ± 3 w, d	37 ± 3 w, d	37 ± 3 w, d	ScI_4^-
			54 ± 3 vw, d	54 ± 3 w, d	54 ± 3 w,d	54 ± 3 w, d	ScI_4^-
67 ± 2 m, d	67 ± 2 m, d	67 ± 2 w, d					ScI_6^{3-}
		109 ± 1 vw, p	109 ± 1 vw, p	109 ± 1 w, p	109 ± 1 w, p	109 ± 1 m, p	$Sc_2I_9^{3-}$
120 ± 1 vs, p	119 ± 1 vs, p	119 ± 1 vs, p	119 ± 1 vs, p	119 ± 1 s, p	119 ± 1 s, p	119 ± 1 s, p	ScI_6^{3-}
	129 ± 1 sh	120 ± 1 m, p	129 ± 1 s, p	129 ± 1 vs, p	129 ± 1 vs, p	129 ± 1 vs, p	ScI_4^-
		220 ± 2 vw, p	220 ± 2 w, b, p	220 ± 2 w, b, p	220 ± 2 w, b, p	220 ± 2 w, b, p	$Sc_2I_9^{3-}$

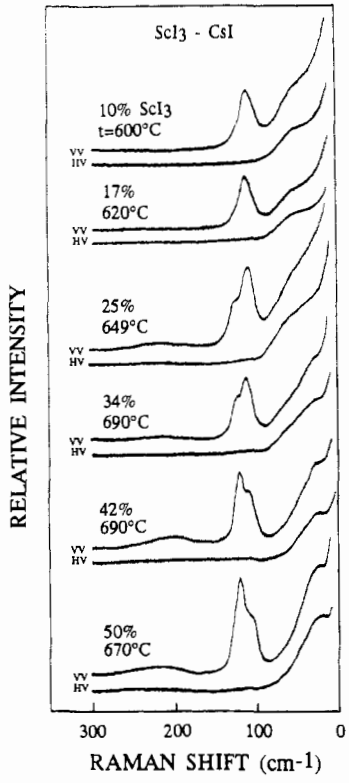

Figure 3. Concentration-dependent Raman spectra of molten ScI_3–CsI mixtures. λ_0 = 6471 Å, spectral slit width; ssw = 5 cm^{-1}, time constant; τ = 0.03 s, scan rate; sr = 0.5 cm^{-1}/s. I_{VV} indicates that incident and scattered radiation is polarized perpendicular to the scattering plane. I_{HV} indicates that incident radiation is polarized in the scattering plane and the scattered radiation is analyzed perpendicular to the scattering plane.

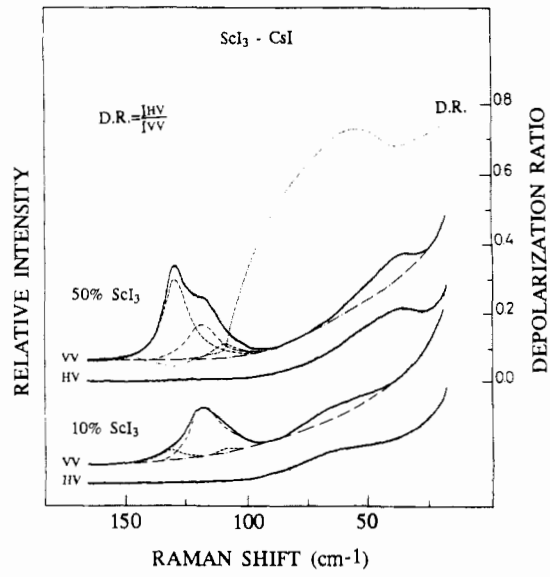

Figure 4. Deconvolution of Raman spectra of ScI_3–CsI melts, at 10 mol % ScI_3 (t = 600 °C) and 50 mol % ScI_3 into Lorentzian curves. DR is the Linear Depolarization Ratio Raman spectrum for the 50 mol % ScI_3 mixture, λ_0 = 6471 Å, ssw = 5 cm^{-1}, τ = 0.03 s, and sr = 0.5 cm^{-1}/s.

The $^2/_3$ compound appears first in the system ScI_3–RbI in coexistence with the $^1/_3$ compound. In the ScI_3–CsI system, the $^2/_3$ compound becomes the most pronounced species. In all known phase diagrams of the type LnI_3–AI (Ln = Sc, Y, La, ..., Lu; A = Na, K, Rb, Cs)[4-6] the $^2/_3$ compound seems to be most pronounced in the ScI_3–CsI system.

Raman Spectra of Melts. Raman spectra have been obtained from a series of samples with concentrations extending from 10 to 60 mol % of ScI_3. In Table I, the Raman frequencies observed for all the concentrations studied, together with their intensity and polarization characteristics, are listed. A comparison of the relative intensities of a particular band among the spectra obtained at different ScI_3 concentrations is not possible because of gradual darkening of the red melts with increasing ScI_3 mole fraction. The dark melts absorbed partially both the incident radiation and the Raman signal, and thus no concentration above 60 mol % ScI_3 could be studied. When inspecting the spectra in Figure 3, it becomes apparent that the spectral changes are described by Raman bands having definite frequencies and dependent relative intensities. Two main bands at ~130 and ~120 cm^{-1} were observed. The 120-cm^{-1} band predominates in the spectra at high CsI mole fraction while the intensity of the 130-cm^{-1} band increases with increasing ScI_3 mole fraction. This indicates the presence of species equilibria in the melt mixtures, as for the $AlCl_3$–ACl systems,[21] rather than gradual structural changes which are expressed by a continuous shift of the Raman bands, as in the case of the YCl_3–ACl (A = Cs, K, Li) systems.[15] However the absence of any abrupt change in the spectra throughout the whole concentration range studied indicates the presence of equilibrium species at all melt compositions. For each spectrum the relative intensities of the Raman bands shown in Figure 3 did not change within 70 °C above melting.

In Figure 4 a portion of the Raman spectra measured for the 50 mol % ScI_3 mixture is deconvoluted into Lorentzian curves and compared with the 10 mol % spectrum. To a good approximation, there are three polarized bands within the composite band for the 50% mixtures centered at 129, 119, and 109 cm^{-1}. The presence of the weak peak at ~110 cm^{-1} is also confirmed by the calculation of the linear depolarization ratio (DR = I_{HV}/I_{VV}) which is presented by a dotted line in Figure 4 and shows an abrupt change of slope at ~110 cm^{-1}.[22] The 10 mol % in ScI_3 spectrum is dominated by a polarized band at 119 cm^{-1} while two weaker polarized bands at 130 and 110 cm^{-1} could be deconvoluted by Lorentzian analysis.

It can be also observed in Figure 4 that the Reyleigh wing decays in a completely different way for the two compared mixtures. For the 50% spectrum, the asymmetric depolarized band probably consists of two bands centered at ~37 and ~54 cm^{-1}, while for the 10% spectrum a more symmetric depolarized band is present at ~67 cm^{-1}. Another characteristic of the spectra rich in ScI_3 is the appearance of a polarized band at ~220 cm^{-1} whose intensity increases with increasing ScI_3 composition.

All these observations are best interpreted as indicating that at *least* two different species are present in these mixtures. One

(21) Begun, G. M.; Boston, C. R.; Torsi, G.; Mamantov, G. *Inorg. Chem.* **1971**, *10*, 886.

(22) The combination of Raman and depolatization ratio spectra for a better determination of the number of bands present in a melt has been illustrated previously for melts[15] and amorphous materials: Papatheodorou, G. N.; Solin, S. A. *Phys. Rev. B* **1976**, *13*, 1741.

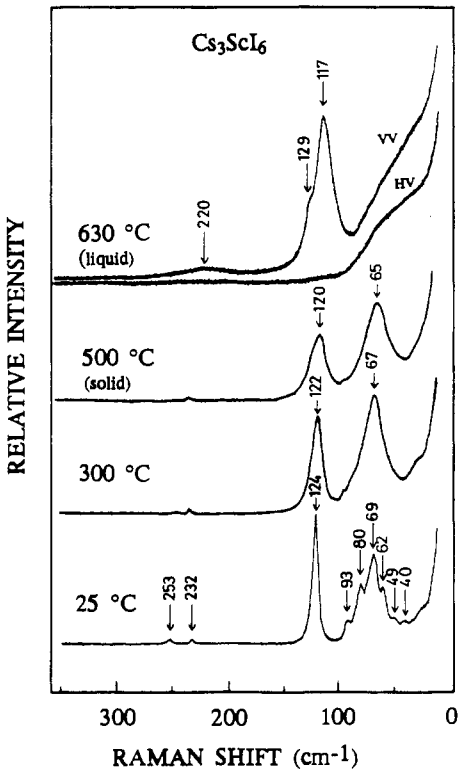

Figure 5. Raman spectra of polycrystalline and molten ScI_3·3CsI. λ_0 = 6471 Å, ssw = 4 cm^{-1}, τ = 0.03 s, and sr = 0.5 cm^{-1}/s.

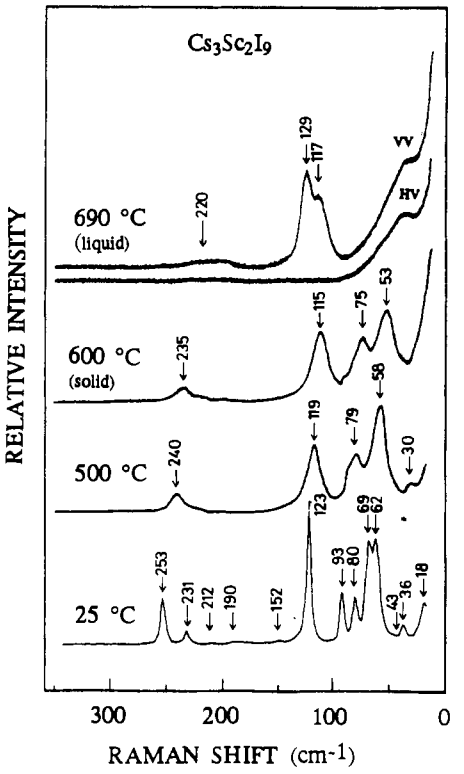

Figure 6. Raman spectra of polycrystalline and molten 2ScI_3·3CsI. λ_0 = 6471 Å, ssw = 4 cm^{-1}, τ = 0.03 s, and sr = 0.5 cm^{-1}/s.

is favored in solutions rich in CsI while the other(s) dominate the ScI_3-rich mixtures.

Raman Spectra of the Solids. Raman spectra of the Cs_3ScI_6 and $Cs_3Sc_2I_9$ polycrystalline compounds have been measured from ambient temperature up to the melting point (Figures 5 and 6). The crystal structure of $Cs_3Sc_2I_9$ is known (D_{6h}^4-$P6_3/mmc$)[23] but

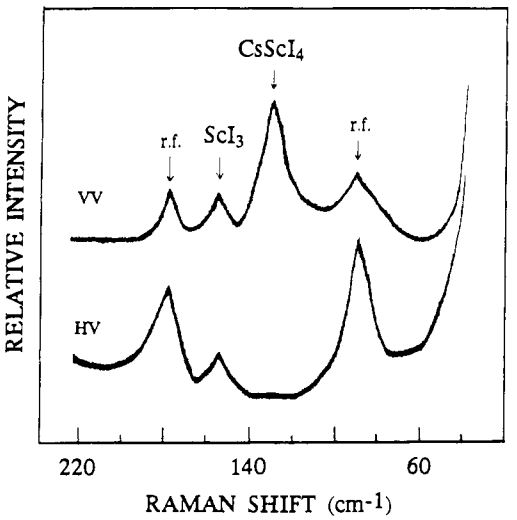

Figure 7. Raman spectra of the gas phase over an equimolar ScI_3–CsI mixture at 800 °C. λ_0 = 4880 Å, ssw = 9 cm^{-1}, τ = 6 s, and sr = 0.05 cm^{-1}/s.

no data are available for the Cs_3ScI_6 compound. In the unit cell of $Cs_3Sc_2I_9$ there are two $Sc_2I_9^{3-}$ units, which consist of two octahedra bound by a face and possess an approximately D_{3h} symmetry. This ion is isostructural with a number of $M_2X_9^{3-}$ (M = Cr,[24] W,[25] Ti,[26] Mo[27]) ions which have been also investigated by vibrational spectroscopy (M = Cr,[28,29] W,[29] Ti,[30] Mo[31]). Factor group analysis for the $Cs_3M_2X_9$ solid and correlation tables for the $M_2X_9^{3-}$ ion have been also reported.[28,29,31] If the low-frequency acoustic and rotatory modes are ignored, 18 Raman (13 internal, 5 lattice) modes are expected for the $Cs_3M_2X_9$ solids with D_{6h}^4 symmetry, from which 13 are observed in the polycrystalline $Cs_3Sc_2I_9$ spectra (Figure 6). For the $Sc_2I_9^{3-}$ molecular ion, the 13 Raman active vibrations are distributed as follows: $\Gamma_R(Sc_2I_9^{3-})$ = 4A′ + 5E′ + 4E″.

Figures 5 and 6 show that the Raman bands of both solids undergo a temperature-induced broadening the shifting toward lower frequencies. The number of main bands observed *below melting* are 4 for $Cs_3Sc_2I_9$ and 2 for Cs_3ScI_6. The band at ~120 cm^{-1} appears to be common for both solids and is preserved upon melting. The half-width of this band increases with temperature from ~3 cm^{-1} at 25 °C to ~20 cm^{-1} below the melting point. It is noteworthy that the high-temperature Raman spectrum of solid Cs_3ScI_6 is very similar to the spectra of A_3YCl_6 and A_3LaCl_6 (A = K, Cs)[15,17] compounds, which at temperatures below melting also show two bands attributed to the ν_1 (A_{1g}) and ν_5(T_{2g}) vibrational modes of the $LnCl_6^{3-}$ octahedron [$\Gamma_R(LnCl_6^{3-}) = A_{1g} + E_g + T_{2g}$]. It is thus reasonable to assume that the two predominant Raman bands of the Cs_3ScI_6 compound are due to the internal modes of an octahedral ScI_6^{3-}-like species, with ν_1 ~120 cm^{-1}. Two such species bound by a face form $Sc_2I_9^{3-}$, having three bridging and six terminal iodines. The high-frequency (~253 cm^{-1}) Raman band of the $Cs_3Sc_2I_9$ solid, which exhibits a fast red shift with increasing temperature, is assigned to the scandium–iodine terminal stretching of the $Sc_2I_9^{3-}$ species. The ~123-cm^{-1} band is either the bridging stretch or the terminal bend. Figures 5 and 6 show that there is no overall direct correlation of the liquid and the solid spectra. The polarized bands at ~220, 129, and 117 cm^{-1} appear with different relative intensity in both

(23) Meyer, G.; Corbett, J. D. *Inorg. Chem.* **1981**, *20*, 2627.

(24) Wessel, G. J.; Ijdo, D. J. W. *Acta Crystallogr.* **1957**, *10*, 466.
(25) Watson, W. H.; Waser, J. J. *Acta Crystallogr.* **1958**, *11*, 689.
(26) Saillant, R.; Wentworth, R. A. D. *Inorg. Chem.* **1968**, *7*, 1606.
(27) Saillant, R.; Jackson, R. B.; Streib, W. E.; Folting, K.; Wentworth, R. A. D. *Inorg. Chem.* **1971**, *10*, 1453.
(28) Ziegler, R. J.; Risen, W. M. *Inorg. Chem.* **1972**, *11*, 2796.
(29) Black, J. D.; Dunsmuir, J. T. R.; Forrest, I. W.; Lane, A. P. *Inorg. Chem.* **1975**, *14*, 1257.
(30) Briat, B.; Kahn, O.; Morgenstern-Badarau, I.; Rivoal, J. C., *Inorg. Chem.* **1981**, *20*, 4193.
(31) Smith, P. W.; Stranger, R. *Aust. J. Chem.* **1986**, *39*, 1269.

Table II. Vibrational Frequencies (cm^{-1}) Attributed to the Species ScI_6^{3-} and ScI_4^- in the Molten ScI_3–CsI Mixtures with Concentrations of 10–50 mol % ScI_3

ScI_6^{3-}		ScI_4^-	
assignt	freq	assignt	freq
$\nu_1(A_{1g})$	119 ± 1	$\nu_1(A_1)$	129 ● 1
$\nu_2(E_g)$	67 ± 2	$\nu_2(E)$	37 ● 3
$\nu_5(T_{2g})$	(80[a])	$\nu_4(T_2)$	54 ± 3

[a] Calculated from the relation $\nu_1^2 \approx \nu_2^2 + (3/2)\nu_5^2$.[37]

melts but only one of them at 117 cm^{-1} has a counterpart in the solid.

Raman Spectra of the Gas Phase. Raman spectra of vapors over the equimolar ScI_3–CsI mixture have been obtained at 800 °C (Figure 7). The cell contained ~3 atm of mercury metal vapor pressure to suppress fluorescence as suggested by Maroni and Cunningham.[32] A strong polarized band is observed at 127 cm^{-1} and is assigned to the ν_1 vibration of the "tetrahedral" ScI_4 in the $CsScI_4$ molecule. Mass spectrometry has revealed the existence of $AScI_4$ gas molecules in the equilibrium vapors over ScI_3–AI (A = Li, Na, Cs) mixtures.[33,34] In the $AScI_4$ molecule, scandium is presumably tetrahedrally coordinated. Because of the very weak Raman signal, the spectrum had to be scanned slowly and the time needed for each run was about 75 min. Unfortunately ScI_3 attacks the quartz cell, producing some Si–Sc–I species, the quantity being time dependent. In Figure 7, two resonance fluorescence bands are present, centered at 88 and 153 cm^{-1}, respectively. (The peak at 176 cm^{-1} is an overtone of the 88-cm^{-1} peak). The intensity of the band at 88 cm^{-1} is strongly time dependent, leading to the conclusion that the species is constantly produced through a reaction between ScI_3 and the quartz cell. The presence of Hg in the cell delays the appearance of this resonance fluorescence band,[32] probably by collision-induced deactivation of the unknown Si–Sc–I species. The intensity of the band at 153 cm^{-1} is not strongly affected by the presence of Hg in the cell, but neither does it seem to be time dependent. Therefore it is reasonable to assume that it is due to ScI_3, and it is attributed to a resonance fluorescence of the ν_1 ScI_3 vibration. The 153-cm^{-1} band is very close to the literature values for the ν_1 vibrations of the planar AlI_3, GaI_3, and InI_3 molecules which are at 156, 147, and 151 cm^{-1}, respectively.[35] In the I_{HV} spectrum, obtained directly after the I_{VV}, the intensity of the resonance fluorescence bands at 88 and 176 cm^{-1} is increased and the polarized band at 128 cm^{-1} cannot be observed. The other and weaker depolarized Raman bands expected for the ScI_4 tetrahedra were not observed as in cases of other vapor Raman spectra of similar molecules (i.e: $InAlX_4$, $InInX_4$ (X = Cl, Br)).[36]

The Melt Structure. The 127-cm^{-1} frequency for the ν_1 vibration of the "tetrahedral" ScI_4 in the vapor species can be correlated to the band at 130 cm^{-1} in the molten-phase spectra. In the $InAlX_4$ systems,[36] a similar frequency shift has been observed for $AlCl_4^-$ and $AlBr_4^-$ species on going from the gas- to the liquid-phase spectra (e.g. 205 and 208 cm^{-1} for the ν_1 vibration of $AlBr_4^-$ in the gas phase and the liquid phase, respectively). Consequently the 129-cm^{-1} polarized band of the melt can be assigned to the ν_1 vibrational mode of a tetrahedral ScI_4^- species. Since the depolarized bands at ~37 and ~54 cm^{-1} increase in intensity parallel to the 129-cm^{-1} band, these bands can be tentatively assigned to the ν_2 and ν_4 tetrahedral modes, while the weak broad ν_3 band expected[21] at about 300 cm^{-1} cannot be observed. The band at 119 cm^{-1}, which is the only strong polarized band for CsI-rich mixtures, is tentatively assigned to the ν_1 mode of an "octahedral" ScI_6^{3-} species. The presence of this species is in agreement with the melt structures proposed in the literature for alkali-metal halide rich LnX_3–AX systems.[13,15-17] The depolarized band at 70 cm^{-1} can be tentatively assigned to the ν_2 octahedral vibration, while the ν_5 mode, usually present as a weak shoulder band, cannot be observed[15] but can easily be calculated[37] (see Table II). The frequencies of the discussed Raman bands are in good correspondence with the ones observed for the $AlF_6^{3-} \rightleftharpoons AlF_4^- + 2F^-$ equilibrium in molten cryolite-type mixtures.[38] However, the tetrahedral–octahedral equilibrium

$$ScI_6^{3-} \rightleftharpoons ScI_4^- + 2I^- \qquad (1)$$

cannot account for the existence of the polarized band at ~220 cm^{-1} (Figures 3 and 4) and the convoluted polarized band at ~110 cm^{-1}. The band at 220 cm^{-1} has a more pronounced intensity for ScI_3-rich mixtures, and it is tentatively attributed (together with the 110-cm^{-1} band) to a binuclear Sc species. Two obvious possibilities for such species are the $Sc_2I_9^{3-}$ and the $Sc_2I_7^-$ ions. The former is an entity present in the $Cs_3Sc_2I_9$ solid that has a weak band in the 220–230-cm^{-1} region. As the ScI_3 content is increased in the melt mixture, the ScI_6^{3-} could form ScI_4^- or/and further associate and form polynuclear Sc (i.e. $Sc_2I_9^{3-}$, $Sc_3I_{12}^{3-}$, etc.) species having a number of ScI_6^{3-} octahedra bound by faces. On the other hand, the $Sc_2I_7^-$ species having two ScI_4^- tetrahedra bridged with an iodine is more likely, as in the case of the $Al_2X_7^-$ species,[21] to have an optimum composition for formation near 66 mol % ScI_3. Furthermore the two polarized bands measured for the $Al_2I_7^-$ ion[21] at 288 and 137 cm^{-1} scale reasonably to the ~220 and ~110-cm^{-1} bands and could be attributed to the $Sc_2I_7^-$ ion. In the MX_3–AX mixtures of trivalent salts forming molecular melts (e.g., AlX_3, GaX_3[39]), the $M_2X_7^-$ ion provides the structural link between the isolated MX_4^- tetrahedral (at 50 mol % MX_3) and the doubly bridged tetrahedra M_2X_6 molecule of the pure MX_3 melt. For ionic-like LnX_3 melts, which preserve the local coordination of the solid (e.g. YCl_3[15]), the structure of the LnX_3–AX mixtures favors the formation of $Ln_2X_9^{3-}$, $Ln_3X_{12}^{3-}$, etc. ions which preserve the "octahedral" LnX_6^{-3} coordination throughout the different mixture compositions. In the case of ScI_3, the existence of a Sc_2I_6 molecular melt is doubtful in view of both the high melting/boiling point and the measured electrical conductivities of the lanthanide iodides, having values in the order of magnitude of those for ionic melts.[40] It is thus more likely that the third species in the ScI_3–CsI mixtures is the $Sc_2I_9^{3-}$ ion.

Conclusions. The phase diagram of the ScI_3–CsI system has been determined. The structure of the ScI_3–CsI binary molten mixtures can be described through two chemical equilibria. The main equilibrium, for the concentration range 10–50 mol % ScI_3, is between ScI_4^- and ScI_6^{3-} species. At the same time a dimeric species, possibly $Sc_2I_9^{3-}$, is formed. The equilibrium involving the dimeric species is more pronounced at higher ScI_3 concentrations. The structure of the melt is related to the structure of the gas phase through the ScI_4^- species.

Acknowledgment. This work has been supported by the Hellenic General Secretariat of Research and Technology—International Collaboration Program. Many thanks are given to Drs S. Philipakis and V. Psycharis (NRC-Democritos, Athens) for their help in the X-ray powder diffraction analysis and to Prof. T. Østvold (NTH-Trondheim) for comments on the manuscript.

Registry No. ScI_3, 14474-33-0; CsI, 7789-17-5; Cs_3ScI_6, 74462-99-0; $Cs_3Sc_2I_9$, 74472-54-1; ScI_6^{3-}, 136184-94-6; ScI_4^-, 136235-67-1.

Supplementary Material Available: Table A, giving phase transitions for the ScI_3–CsI system from DTA measurements, and Table B, giving X-ray diffraction data for ScI_3, ScI_3·3CsI, and $2ScI_3$·3CsI (2 pages). Ordering information is given on any current masthead page.

(32) Maroni, V. A.; Cunningham, P. T. *Appl. Spectrosc.* **1973**, *27*, 428.
(33) Hirayama, C.; Castle, P. M.; Liu, C. S.; Zollweg, R. J. *J. Illum. and Eng. Soc.* **1977**, 209.
(34) Hilpert, K.; Miller, M. *J. Electrochem. Soc.* **1990**, *137*, 1618.
(35) Beattie, I. R.; Horder, J. R. *J. Chem. Soc. A* **1969**, 2655.
(36) Radloff, P. L.; Papatheodorou, G. N. *J. Chem. Phys.* **1980**, *72*, 992.
(37) Yost, D. M.; Steffins, C. C.; Gross, S. T. *J. Chem. Phys.* **1934**, *2*, 311.
(38) Gilber, B.; Mamantov, G.; Begun, G. M. *J. Chem. Phys.* **1975**, *62*, 950.
(39) Beattie, I. R.; Gilson, T.; Ozin, G. A. *J. Chem. Soc. A* **1968**, 813.
(40) Janz; et al. *J. Phys. Chem. Ref. Data* **1977**, *6* (2).